

LATTICE CALCULATION OF THE GLUON PROPAGATOR AND THE STRANGENESS MAGNETIC MOMENT OF THE NUCLEON

Anthony G. Williams

CSSM and Department of Physics and Mathematical Physics

University of Adelaide, Australia 5005

`awilliam@physics.adelaide.edu.au`

`http://www.physics.adelaide.edu.au/cssm`

ABSTRACT

This contribution summarizes a presentation combining two topics in lattice QCD. Firstly, the gluon propagator in Landau gauge is calculated in quenched QCD on a large $(32^3 \times 64)$ lattice at $\beta = 6.0$. New structure seen in the infrared region survives conservative cuts to the lattice data, and serves to exclude a number of models that have appeared in the literature. Secondly, I report on a recent lattice QCD calculation of the strangeness magnetic moment of the nucleon. The result is $G_M^s(0) = -0.36 \pm 0.20$. The strangeness Sachs electric mean-square radius $\langle r_s^2 \rangle_E$ was also found to be small and negative.

1. Introduction

Here I summarize the central results described in a single long parallel session talk, which was comprised of two distinct studies of lattice QCD. The first of these is concerned with the direct lattice calculation of the Landua gauge nonperturbative gluon propagator, an understanding of which is central to our understanding of the nature of confinement. The second topic is a lattice calculation of the strangeness magnetic moment of the nucleon. Different confining quark models predict a variety of results for this quantity and so lattice calculations provide a benchmark against which we can test our understanding of hadron structure.

2. Lattice Calculation of the Gluon Propagator

2.1. Motivation

The infrared behaviour of the gluon propagator is important for an understanding of confinement. Previous conjectures range from a strong divergence^{1,2} to a propagator that vanishes in the infrared.^{3,4} Lattice QCD should in principle be able to resolve this issue by first-principles, model-independent calculations. However, lattice studies have been inconclusive up to now,^{5,6} since they have not been able to access sufficiently low momenta. The lower limit of the available momenta on the lattice is given by

$q_{\min} = 2\pi/L$, where L is the length of the lattice. Here we will report results using a lattice with a length of 3.3 fm in the spatial directions and 6.7 fm in the time direction. This gives us access to momenta as small as 400 MeV.

2.2. Summary of Formalism

The gluon field A_μ can be extracted from the link variables $U_\mu(x)$ using $U_\mu(x) = e^{ig_0 a A_\mu(x + \hat{\mu}/2)} + \mathcal{O}(a^3)$. Inverting and Fourier transforming this, we obtain

$$\begin{aligned} A_\mu(\hat{q}) &\equiv \sum_x e^{-i\hat{q} \cdot (x + \hat{\mu}/2)} A_\mu(x + \hat{\mu}/2) \\ &= \frac{e^{-i\hat{q}_\mu a/2}}{2ig_0 a} \left[\left(U_\mu(\hat{q}) - U_\mu^\dagger(-\hat{q}) \right) - \frac{1}{3} \text{Tr} \left(U_\mu(\hat{q}) - U_\mu^\dagger(-\hat{q}) \right) \right], \end{aligned} \quad (1)$$

where $U_\mu(\hat{q}) \equiv \sum_x e^{-i\hat{q}x} U_\mu(x)$ and $A_\mu(\hat{q}) \equiv t^a A_\mu^a(\hat{q})$. The available momentum values \hat{q} are given by $\hat{q}_\mu = 2\pi n_\mu / (aN_\mu)$, $n_\mu = 0, \dots, N_\mu - 1$, where N_μ is the number of points in the μ direction. The gluon propagator $D_{\mu\nu}^{ab}(\hat{q})$ is defined as $D_{\mu\nu}^{ab}(\hat{q}) = \langle A_\mu^a(\hat{q}) A_\nu^b(-\hat{q}) \rangle / V$. The Landau gauge propagator in the continuum has the structure $D_{\mu\nu}^{ab}(q) = \delta^{ab} [\delta_{\mu\nu} - (q_\mu q_\nu / q^2)] D(q^2)$. At tree level, $D(q^2)$ will have the form $D^{(0)}(q^2) = 1/q^2$. On the lattice, this becomes

$$D^{(0)}(\hat{q}) = 1 / \sum_\mu \left(\frac{2}{a} \sin \frac{\hat{q}_\mu a}{2} \right)^2. \quad (2)$$

Since QCD is asymptotically free, we expect that up to logarithmic corrections, $q^2 D(q^2) \rightarrow 1$ in the ultraviolet. Hence we define the new momentum variable q by $q_\mu \equiv (2/a) \sin(\hat{q}_\mu a/2)$ and work with this throughout. The (bare) lattice gluon propagator is related to the renormalised continuum propagator $D_R(q; \mu)$ via $D^L(qa) = Z_3(\mu, a) D_R(q; \mu)$. The renormalisation constant $Z_3(\mu, a)$ can be found by imposing a momentum subtraction renormalisation condition $D_R(q)|_{q^2=\mu^2} = 1/\mu^2$. The asymptotic behaviour of the renormalised gluon propagator in the continuum is given to one-loop level by $D_R(q) \equiv D_{\text{bare}}(q)/Z_3 = (1/q^2) [(1/2) \ln(q^2/\Lambda^2)]^{-d_D}$ with $d_D = (39 - \xi - 4N_f)/[4(33 - 2N_f)] = 13/44$, where both the gauge parameter ξ and the number of fermion flavours N_f are zero in this calculation.

2.3. Simulation Parameters, Finite Size Effects and Anisotropies

We have analysed three lattices, with different values for the volume and lattice spacing. The details are given in Table 1. In the following, we are particularly interested in the deviation of the gluon propagator from the tree level form. We will therefore factor out the tree level behaviour and plot $q^2 D(q^2)$ rather than $D(q^2)$ itself.

Fig. 1 shows the gluon propagator as a function of qa for the small and large lattices, with momenta in different directions plotted separately. For low momentum values on the small lattice, there are large discrepancies due to finite size effects between points representing momenta along the time axis and those representing momenta along the spatial axes. These discrepancies are absent from the data from the large lattice, indicating that finite size effects here are under control.

Name	β	a_{st}^{-1} (GeV)	Volume	N_{conf}	$a\hat{q}_{\text{Max}}$	$ \partial_\mu A_\mu $
Small	6.0	1.885	$16^3 \times 48$	125	$2\pi/4$	$< 10^{-6}$
Large	6.0	1.885	$32^3 \times 64$	75	$2\pi/4$	$< 10^{-6}$
Fine	6.2	2.63	$24^3 \times 48$	223	$2\pi/4$	$< 10^{-6}$

Table 1. Simulation parameters

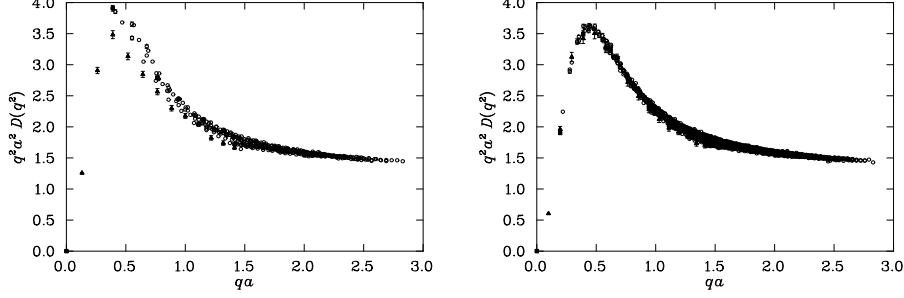


Fig. 1. Componentwise data, for the small lattice (left) and the large lattice (right). The filled triangles denote momenta directed along the time axis, while the filled squares denote momenta directed along one of the spatial axes.

However, at higher momenta, there are anisotropies which remain for the large lattice data, and which are of approximately the same magnitude for the two lattices. In order to eliminate these anisotropies, which arise from large momenta (i.e., finite lattice spacing errors), we select momenta lying within a cylinder of radius $\Delta\hat{q}a = 2 \times 2\pi/32$ along the 4-dimensional diagonals in order to distribute large momenta across the four momentum components.⁷

2.4. Scaling behaviour

Since the renormalised propagator $D_R(q; \mu)$ is independent of the lattice spacing, we can derive a simple, q -independent expression for the ratio of the unrenormalised lattice gluon propagators at the same value of q :

$$\frac{D_c(qa_c)}{D_f(qa_f)} = \frac{Z_3(\mu, a_c)D_R(q; \mu)/a_c^2}{Z_3(\mu, a_f)D_R(q; \mu)/a_f^2} = \frac{Z_c}{Z_f} \frac{a_f^2}{a_c^2}, \quad (3)$$

where the subscript f denotes the finer lattice ($\beta = 6.2$ in this study) and the subscript c denotes the coarser lattice ($\beta = 6.0$). We can use this relation to study directly the scaling properties of the lattice gluon propagator by matching the data for the two values of β . This matching can be performed by adjusting the values for the ratios $R_Z = Z_f/Z_c$ and $R_a = a_f/a_c$ until the two sets of data lie on the same curve. Fig. 2 shows the data for both lattice spacings as a function of qa before shifting. This

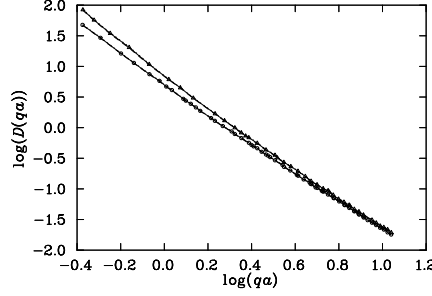


Fig. 2. The dimensionless, unrenormalised gluon propagator as a function of $\ln(qa)$ for the two values of β . The triangles denote the data for the small lattice at $\beta = 6.0$, while the circles denote the data for $\beta = 6.2$.

procedure gives us an estimate of $R_a = 0.745^{+32}_{-37}$, which is fully compatible with the string-tension value⁸ of 0.716 ± 0.040 . The corresponding estimate for the ratio of the renormalisation constants is $R_Z = 1.038^{+26}_{-21}$.

2.5. Model Fits

We have demonstrated scaling in our lattice data over the entire range of q^2 considered, and will now proceed with model fits. The following functional forms have been considered:

$$D(q^2) = \frac{Zq^2}{q^4 + M^4} \left(\frac{1}{2} \ln \frac{q^2 + M^2}{M^2} \right)^{-d_D} \quad (\text{Gribov}^3) \quad (4)$$

$$D(q^2) = Z \frac{q^2}{q^4 + 2A^2q^2 + M^4} \left(\frac{1}{2} \ln \frac{q^2 + M^2}{M^2} \right)^{-d_D} \quad (\text{Stingl}^4) \quad (5)$$

$$D(q^2) = \frac{Z}{(q^2)^{1+\alpha} + M^2} \quad (\text{Marenzoni et al}^6) \quad (6)$$

$$D(q^2) = Z \left[(q^2 + M^2(q^2)) \ln \frac{q^2 + 4M^2(q^2)}{\Lambda^2} \right]^{-1} \quad (\text{Cornwall}^9) \quad (7)$$

$$\text{where} \quad M(q^2) = M \left\{ \ln \frac{q^2 + 4M^2}{\Lambda^2} / \ln \frac{4M^2}{\Lambda^2} \right\}^{-6/11}$$

$$D(q^2) = Z \left(\frac{A}{(q^2 + M_{\text{IR}}^2)^{1+\alpha}} + \frac{1}{q^2 + M_{\text{UV}}^2} \left(\frac{1}{2} \ln \frac{q^2 + M_{\text{UV}}^2}{M_{\text{UV}}^2} \right)^{-d_D} \right) \quad (8)$$

$$D(q^2) = Z \left(\frac{A}{(q^2)^{1+\alpha} + (M_{\text{IR}}^2)^{1+\alpha}} + \frac{1}{q^2 + M_{\text{UV}}^2} \left(\frac{1}{2} \ln \frac{q^2 + M_{\text{UV}}^2}{M_{\text{UV}}^2} \right)^{-d_D} \right) \quad (9)$$

$$D(q^2) = Z \left(Ae^{-(q^2/M_{\text{IR}}^2)^\alpha} + \frac{1}{q^2 + M_{\text{UV}}^2} \left(\frac{1}{2} \ln \frac{q^2 + M_{\text{UV}}^2}{M_{\text{UV}}^2} \right)^{-d_D} \right) \quad (10)$$

We have also considered¹⁰ special cases of the three forms (8)–(10), with $M_{\text{IR}} = M_{\text{UV}}$ or with specific values for the exponent α . Equations (4) and (5) are modified in order to exhibit the appropriate one-loop asymptotic behaviour. Models (8) and (9) are constructed as generalisations of (6) with the correct dimension and asymptotic

Model	χ^2/dof	Z	A	M_{IR}	M_{UV} or Λ	α
4	1972	2.19^{+31}_{-15}		0.23^{+14}_{-1}		
5	1998	2.2	0	0.23		
6	163	2.41^{+0}_{-12}		0.14^{+4}_{-14}		0.29^{+6}_{-2}
7	50.3	6.5^{+7}_{-9}		0.24^{+3}_{-16}	0.27^{+7}_{-7}	
8	2.96	1.54^{+10}_{-20}	1.24^{+21}_{-21}	0.46^{+2}_{-14}	0.96^{+47}_{-17}	1.31^{+16}_{-43}
8; $M_{\text{IR}} = M_{\text{UV}}$	3.73	1.71^{+9}_{-0}	0.84^{+0}_{-29}	0.48^{+2}_{-17}		1.52^{+12}_{-37}
9	1.57	1.78^{+45}_{-20}	0.49^{+17}_{-6}	0.43^{+5}_{-1}	0.20^{+37}_{-19}	0.95^{+7}_{-5}
9; $M_{\text{IR}} = M_{\text{UV}}$	4.00	1.62^{+3}_{-4}	0.58^{+5}_{-1}	0.40^{+9}_{-2}		0.92^{+17}_{-1}
10	47	2.09^{+30}_{-12}	29^{+166}_{-2}	0.22^{+0}_{-16}	0.14^{+11}_{-10}	0.49^{+0}_{-16}

Table 2. Parameter values for fits to models (4)–(10). The values quoted are for fits to the entire set of data. The errors denote the uncertainties in the last digit(s) of the parameter values which result from varying the fitting range. The fitting ranges considered when evaluating the uncertainties are those with a minimum of 40 points included and with the minimum value for qa no larger than 1.03 (point number 40).

behaviour. All models were fitted to the large lattice data using the cylindrical cut. The lowest momentum value was excluded, as the volume dependence of this point could not be assessed. In order to balance the sensitivity of the fit between the high- and low-momentum region, nearby data points within $\Delta(qa) < 0.05$ were averaged. χ^2 per degree of freedom and parameter values for fits to all these models are shown in Table 2. It is clear that model (9) accounts for the data better than any of the other models. The best fit to this model is illustrated in Fig. 3.

2.6. Summary of Numerical Results

We have evaluated the gluon propagator on an asymmetric lattice with a large physical volume. By studying the anisotropies in the data, and comparing the data with those from a smaller lattice, we have been able to conclude that finite size effects are under control on the large lattice. A clear turnover in the behaviour of $q^2 D(q^2)$ has been observed at $q \sim 1\text{GeV}$, indicating that the gluon propagator diverges less rapidly than $1/q^2$ in the infrared, and may be infrared finite or vanishing. The data are consistent with a functional form $D(q^2) = D_{\text{IR}} + D_{\text{UV}}$, where

$$D_{\text{IR}} = \frac{1}{2} \frac{1}{q^4 + M^4}, \quad (11)$$

$M \sim 1\text{ GeV}$, and D_{UV} is the appropriate asymptotic form. A more detailed analysis¹⁰ of the asymptotic behaviour reveals that the one-loop formula remains insufficient at $q^2 = 50\text{GeV}^2$. Issues for future study include the effect of Gribov copies and of dynamical fermions. We also hope to use improved actions to perform realistic simulations at larger lattice spacings. This would enable us to evaluate the gluon propagator on larger physical volumes, giving access to lower momentum values.

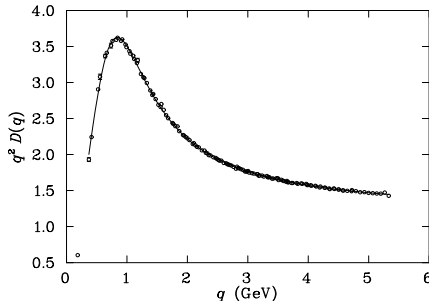


Fig. 3. The gluon propagator multiplied by q^2 , with nearby points averaged. The line illustrates our best fit to the form defined in (9). The fit is performed over all points shown, excluding the one at the lowest momentum value, which may be sensitive to the finite volume of the lattice. The scale is taken from the string tension.⁸

3. Nucleon Strangeness Magnetic Moment

3.1. Motivation

We summarize some recent results¹¹ on nucleon electromagnetic form factors, including the strangeness electric and magnetic form factors. The strangeness content of the nucleon has been a topic of considerable recent interest for a variety of reasons. The studies of nucleon spin structure functions in polarized deep inelastic scattering experiments at CERN and SLAC,¹² combined with neutron and hyperon β decays, have turned up a surprisingly large and negative polarization from the strange quark. In addition, there is a well-known long-standing discrepancy between the pion-nucleon sigma term extracted from the low energy pion-nucleon scattering¹³ and that from the octet baryon masses.¹⁴ This discrepancy can be reconciled if a significant $\bar{s}s$ content in the nucleon^{14,15} is admitted. To address some of these issues, an experiment to measure the neutral weak magnetic form factor G_M^Z via elastic parity-violating electron scattering at backward angles was recently carried out by the SAMPLE collaboration.¹⁶ The strangeness magnetic form factor is obtained by subtracting out the nucleon magnetic form factors G_M^p and G_M^n . The reported value is $G_M^s(Q^2 = 0.1 \text{ GeV}^2) = +0.23 \pm 0.37 \pm 0.15 \pm 0.19$ and does not yet provide a strong constraint on the sign.

Theoretical predictions of $G_M^s(0)$ vary widely. The values from various models and analyses range from -0.75 ± 0.30 in a QCD equalities analysis¹⁷ to $+0.37$ in an $SU(3)$ chiral bag model.¹⁸ While a few give positive values,^{18,19} most model predictions are negative with a typical range of -0.25 to -0.45 . Summaries of these predictions can be found in Refs.^{17,20} A similar situation exists for the strangeness electric mean-square radius $\langle r_s^2 \rangle_E$. A number of the predictions are positive while a few are negative. Elastic $\vec{e}p$ and \vec{e}^4He parity-violation experiments are currently planned at TJNAF²¹ to measure the asymmetry A_{LR} at forward angles to extract $\langle r_s^2 \rangle_E$. Hopefully, they will settle the issue of its sign.

3.2. Numerical Results

The lattice formulation of the electromagnetic and other form factors has been given in detail in the past.^{22,23} Here, we shall concentrate on the DI contribution, where the strangeness current contributes. In the Euclidean formulation, the Sachs EM form factors can be obtained by the combination of two- and three-point functions

$$G_{NN}^{\alpha\alpha}(t, \vec{p}) = \sum_{\vec{x}} e^{-i\vec{p}\cdot\vec{x}} \langle 0 | \chi^\alpha(x) \bar{\chi}^\alpha(0) | 0 \rangle \quad (12)$$

$$G_{NV_\mu N}^{\alpha\beta}(t_f, \vec{p}, t, \vec{q}) = \sum_{\vec{x}_f, \vec{x}} e^{-i\vec{p}\cdot\vec{x}_f + i\vec{q}\cdot\vec{x}} \langle 0 | \chi^\alpha(x_f) V_\mu(x) \bar{\chi}^\beta(0) | 0 \rangle, \quad (13)$$

where χ^α is the nucleon interpolating field and $V_\mu(x)$ the vector current. With large Euclidean time separation, i.e. $t_f - t \gg a$ and $t \gg a$, where a is the lattice spacing,

$$\frac{\Gamma_i^{\beta\alpha} G_{NV_j N}^{\alpha\beta}(t_f, \vec{0}, t, \vec{q})}{G_{NN}^{\alpha\alpha}(t_f, \vec{0})} \frac{G_{NN}^{\alpha\alpha}(t, \vec{0})}{G_{NN}^{\alpha\alpha}(t, \vec{q})} \longrightarrow \frac{\varepsilon_{ijk} q_k}{E_q + m} G_M(q^2), \quad (14)$$

$$\frac{\Gamma_E^{\beta\alpha} G_{NV_4 N}^{\alpha\beta}(t_f, \vec{0}, t, \vec{q})}{G_{NN}^{\alpha\alpha}(t_f, \vec{0})} \frac{G_{NN}^{\alpha\alpha}(t, \vec{0})}{G_{NN}^{\alpha\alpha}(t, \vec{q})} \longrightarrow G_E(q^2), \quad (15)$$

where $\Gamma_i = \sigma_i(1 + \gamma_4)/2$ and $\Gamma_E = (1 + \gamma_4)/2$.

We shall use the conserved current from the Wilson action which, being point-split, yields slight variations on the above forms and these are given in Ref.²³ Our 50 quenched gauge configurations were generated on a $16^3 \times 24$ lattice at $\beta = 6.0$. In the time direction, fixed boundary conditions were imposed on the quarks to provide larger time separations than available with periodic boundary conditions. We also averaged over the directions of equivalent lattice momenta in each configuration; this has the desirable effect of reducing error bars. Numerical details of this procedure are given in Refs.^{23,24} The dimensionless nucleon masses $M_N a$ for $\kappa = 0.154, 0.152$, and 0.148 are $0.738(16)$, $0.882(12)$, and $1.15(1)$ respectively. The corresponding dimensionless pion masses $m_\pi a$ are $0.376(6)$, $0.486(5)$, and $0.679(4)$. Extrapolating the nucleon and pion masses to the chiral limit we determine $\kappa_c = 0.1567(1)$ and $m_N a = 0.547(14)$. Using the nucleon mass to set the scale to study nucleon properties,^{22,24} the lattice spacing $a^{-1} = 1.72(4)$ GeV is determined. The three κ 's then correspond to quark masses of about 120, 200, and 360 MeV respectively.

The strangeness current $\bar{s}\gamma_\mu s$ contribution appears in the DI only. The full details of the extraction can be found in Ref.¹¹ and we satisfy ourselves here by simply quoting the results. We use a monopole form to extrapolate $G_M^s(q^2)$ with nonzero q^2 to $G_M^s(0)$, giving $G_M^s(0) = -0.36 \pm 0.20$. Correlations are taken into account and the error is from jackknifing the fitting procedure. A similar analysis is done for the strange Sachs electric form factor $G_E^s(q^2)$ and we find that $G_E^s(0)$ is consistent with zero as it should be. We find for the electric mean-square radius $\langle r_s^2 \rangle_E = -6 \frac{dG_E^s(q^2)}{dq^2} \big|_{q^2=0} = -0.061 \pm 0.003 \text{ fm}^2$.

Acknowledgments

Financial support from the Australian Research Council is gratefully acknowledged.

References

1. S. Mandelstam, *Phys. Rev.* **D 20**, 3223 (1979)
2. N. Brown and M.R. Pennington, *Phys. Rev.* **D 39**, 2723 (1989)
3. V.N. Gribov, *Nucl. Phys.* **B 139**, 19 (1978); D. Zwanziger, *Nucl. Phys.* **B 378**, 525 (1992)
4. M. Stingl, *Phys. Rev.* **D 34**, 3863 (1986); *Phys. Rev.* **D 36**, 651 (1987)
5. C. Bernard, C. Parrinello, A. Soni, *Phys. Rev.* **D49**, 1585 (1994)
6. P. Marenzoni, G. Martinelli, N. Stella, *Nucl. Phys.* **B 455**, 339 (1995); P. Marenzoni *et al*, *Phys. Lett.* **B 318**, 511 (1993)
7. D.B. Leinweber, J.I. Skullerud, A.G. Williams, and C. Parrinello *Phys. Rev.* **D 58**, 031501 (1998)
8. G.S. Bali and K. Schilling, *Phys. Rev.* **D 47**, 661 (1993)
9. J. Cornwall, *Phys. Rev.* **D 26**, 1453 (1982)
10. D.B. Leinweber, C. Parrinello, J.I. Skullerud, A.G. Williams, in preparation.
11. S.J. Dong, K.F. Liu, and A.G. Williams, hep-ph/9712483, to appear in *Phys. Rev. D*.
12. J. Ashman *et al.*, *Nucl. Phys.* **B328**, 1 (1989); B. Adeva *et al.*, *Phys. Lett.* **B 329**, 399 (1994); K. Abe *et al.*, *Phys. Rev. Lett.* **74**, 346 (1995).
13. J. Gasser, H. Leutwyler, and M.E. Sainio, *Phys. Lett. B* **253**, 252, 260 (1991).
14. T.P. Cheng, *Phys. Rev.* **D 13**, 2161 (1976); **D 38**, 2869 (1988).
15. J. Gasser and H. Leutwyler, *Phys. Rep.* **87**, 77 (1982).
16. B. Mueller *et al.*, SAMPLE Collaboration, *Phys. Rev. Lett.* **78**, 3824 (1997).
17. D. B. Leinweber, *Phys. Rev.* **D 53**, 5115 (1996).
18. S. T. Hong, B. Y. Park, and D. P. Min, nucl-th/9706008.
19. P. Geiger and N. Isgur, *Phys. Rev.* **D 55**, 299 (1997).
20. C. V. Christov *et. al.*, *Prog. Part. Nucl. Phys.* **37**, 1 (1996).
21. Thomas Jefferson Lab. proposals # PR-91-010, M. Finn and P. Souder, spokespersons , # PR-91-017, D. Beck, spokesperson, and # PR-91-004, E. Beise, spokesperson.
22. S.J. Dong, J.-F. Lagaë, and K.-F. Liu, *Phys. Rev. Lett.* **75**, 2096 (1995); *Phys. Rev. D* **54**, 5496 (1996).
23. T. Draper, R. M. Woloshyn, and K. F. Liu, *Phys. Lett.* **234**, 121 (1990); W. Wilcox, T. Draper, and K. F. Liu, *Phys. Rev.* **D 46**, 1109 (1992).
24. K. F. Liu, S. J. Dong, T. Draper, J. M. Wu, and W. Wilcox, *Phys. Rev.* **D 49**, 4755 (1994); K.F. Liu, S.J. Dong, T. Draper, and W. Wilcox, *Phys. Rev. Lett.* **74**, 2172 (1995).